Available online at www.sciencedirect.com

ScienceDirect

Geochimica et Cosmochimica Acta 292 (2021) 78–93

Geochimica et Cosmochimica Acta

www.elsevier.com/locate/gca

An isotope label method for empirical detection of carbonic anhydrase in the calcification pathway of the coccolithophore *Emiliania huxleyi*

Hongrui Zhang [a,b,*], Sonia Blanco-Ameijeiras [a], Brian M. Hopkinson [c], Stefano M. Bernasconi [a], Luz Maria Mejia [a], Chuanlian Liu [b], Heather Stoll [a]

[a] *Department of Earth Sciences, ETH, Zurich, Sonnegstrasse 5, 8092 Zurich, Switzerland*
[b] *State Key Laboratory of Marine Geology, Tongji University, Siping Road 1239, Shanghai 200092, China*
[c] *Department of Marine Sciences, University of Georgia, Athens, GA 30602, USA*

Received 13 February 2020; accepted in revised form 7 September 2020; available online 16 September 2020

Abstract

Coccolithophores are a group of phytoplankton widely distributed in the ocean, which secrete extracellular calcite plates termed coccoliths. Coccoliths have been increasingly employed as an archive for geochemical, ecological and paleoclimate studies in recent years. A robust application of coccolith-based geochemical proxies relies on understanding the carbon acquisition strategies and the pathways of carbon supply for calcification. Carbonic anhydrase (CA) plays important roles in the carbon concentrating mechanism s of aquatic algae and potentially also in calcification. However, it is difficult to independently assess the role of CA in carbon supply for photosynthesis versus calcification. To fill this gap, we explored a new method to detect the CA activity inside coccolithophore. To achieve this, coccolithophores were cultured with oxygen and carbon isotope labeled dissolved inorganic carbon (DIC). By exploiting the different behavior of oxygen and carbon isotopes with (sea)water, this double label method can elucidate the significance of CA activity in the calcification pathway. Application of this method to *Emiliania huxleyi* shows that CA is present in the calcification pathway, and that there is no significant difference in the CA activity between a high and low CO_2 treatment. However, under low CO_2 treatment *E. huxleyi* enhanced the bicarbonate pumping rate on both cell and chloroplast membranes. This novel method could be performed on other species of coccolithophores in the future and have a potential to extend our knowledge on coccolith oxygen isotope vital effects.

Keywords: Coccolithophore; Carbonic anhjydrase; Isotopic labelling; CCM

1. INTRODUCTION

Coccolithophores are key marine unicellular algae that produce an exoskeleton of calcifying plates called coccoliths. The appearance of the first fossil coccoliths in sediment records dates back to ~200 Ma (Bown, 1998), but according to molecular genetic analysis, their ancestor may be as old as 1200 Myr (Medlin et al., 2008). During their long existence on Earth, the environment has greatly varied from warm and high CO_2 conditions to cold and low CO_2 during the late Pleistocene. Since coccolithophores are important players in the marine carbon cycle, it is crucial to understand how they adapted to low CO_2 concentrations and how this adaptation influenced the carbon cycle. A number of geochemical indicators in coccoliths have been proposed

* Corresponding author at: Department of Earth Sciences, ETH, Zurich, Sonnegstrasse 5, 8092 Zurich, Switzerland.
E-mail addresses: hongrui.zhang@erdw.ethz.ch, 103443_rui@tongji.edu.cn (H. Zhang).

https://doi.org/10.1016/j.gca.2020.09.008
0016-7037/

to potentially record different aspects of the past adaptations and evolution of coccolithophore physiology, including carbon isotopic fractionation in coccoliths (Stoll, 2005; Bolton and Stoll, 2013; McClelland et al., 2017; Holtz et al., 2017); boron concentration and isotopic ratio (Stoll et al., 2012; Diez Fernández et al., 2015; Liu et al., 2018); oxygen isotopic fractionation (Ziveri et al., 2003, 2012; Hermoso et al., 2014), and trace element content such as Sr/Ca (Stoll and Schrag, 2001; Müller et al., 2014). For example, modeling of coccolith carbon isotopes suggest that coccolithophores adapted cellular carbon acquisition strategies to compensate for a diminishing diffusive CO_2 supply at least 5–7 Myr ago (Bolton and Stoll, 2013).

A solid interpretation of such geochemical records and the ecological adaptation of coccolithophores rests on understanding the carbon acquisition strategies and the pathways of carbon supply for calcification. Because of the potential for exchange among intracellular carbon pools and cellular pH regulation, geochemical indicators in calcite may also be affected by processes not directly related to calcification, such as photosynthesis and the carbon concentrating mechanism (CCM) inferred to locally enrich CO_2 at the intracellular site of the photosynthetic enzyme RubisCO. In most algae, systems for supplying carbon to photosynthesis require: (a) active transport of dissolved inorganic carbon (DIC), such as HCO_3^-, using energy (ATP or NADPH) either directly or to establish an ion gradient, (b) intracellular carbonic anhydrases (CA) to accelerate interconversion between CO_2 and HCO_3^-, and (c) proton pumps to maintain pH homeostasis following dehydration of HCO_3^- and to optimize CCM efficiency (Hopkinson et al., 2016; Mangan et al., 2016).

Of these processes, here we focus on the role of active HCO_3^-, pumping and the pathways in which CA is operative. In the coccolithophore *Emilianina huxleyi*, active HCO_3^- pumping is inferred to be an important source of carbon to both photosynthesis and calcification, since both rates are reduced by inhibitors of HCO_3^-/Cl-exchanger, Anion Exchange Protein AE1 (Herfort et al., 2002). However, as the AE1 inhibitors are membrane permeable, this result does not diagnose whether HCO_3^- pumping occurs at the cell membrane, intracellular compartments, or both. Modeling the evolution of carbon and oxygen isotope labels in cellular gas fluxes during photosynthesis via Membrane Inlet Mass Spectrometry (MIMS) has shown that in diatoms, diffusive CO_2 uptake is the main source of carbon into the cell, but that HCO_3^- pumping into the chloroplast is a key component of diatoms CCM (e.g. Hopkinson et al., 2011; Hopkinson, 2014). However, in coccolithophores, the cells' dual use of intracellular inorganic carbon for both photosynthesis and calcification, complicates interpretation of MIMS data and requires specific fixed assumptions about the fraction and species of carbon employed for each process (e.g. Kottmeier et al., 2016a,b). In this way, while results from MIMS experiments suggest a significant increase in HCO_3^- pumping into the cell in low CO_2 treatments (Kottmeier et al., 2016b), disequilibrium experiments suggest a modest but constant HCO_3^- flux into the cell regardless of CO_2 (Kottmeier et al., 2014). Although calcification is assumed to be supplied by direct HCO_3^- transport, as well as diffusion of CO_2 into the calcification space, it is unclear if HCO_3^- is transported directly to the coccolith vesicle, or if it is part of a shared carbon pool for photosynthesis.

The role of CA in coccolithophore carbon acquisition is also not well resolved. Extracellular CA, which can maintain equilibrium of DIC species in the diffusive boundary layer outside the cell, is variably present in coccolithophores (Nimer et al., 1994, 1999; Mercado et al., 2009). Membrane impermeable CA inhibitors in *E. huxleyi* suppress photosynthesis only when DIC is below 1 mM, suggesting that extracellular CA is significant only at low DIC (Herfort et al., 2002). At DIC concentrations typical of natural seawater (2 mM), extracellular CA has been directly detected but at low concentrations in *E. huxleyi*, and is suggested to facilitate a greater importance of CO_2, rather than HCO_3^-, transport into the cell (Stojkovic et al., 2013).

The location and activity of intracellular CA has a more significant important effect than external CA on stable carbon and oxygen isotopic composition of dissolved inorganic carbon pools inside the cell (Hopkinson et al, 2011) and is the focus of this contribution. Intracellular CA, key to intracellular carbon supply to the chloroplast and coccolith vesicle, is inferred to also be present in *E. huxleyi*. So far 12 putative CA transcripts in *E. huxleyi* have been identified (Soto et al., 2006; von Dassow et al., 2009). Several of these inferred CA forms have been shown by immunolabeling, to be intracellular in other marine eukaryotes and by analogy are inferred to be intracellular in coccolithophores (Bach et al., 2013). The involvement of one of these intracellular CA in calcification was hypothesized based on a 25-fold up-regulation of the gene *c-EhCA2* transcripts under calcifying versus non-calcifying condition (Soto et al., 2006; Quinn et al., 2006). However, other syntheses of CA upregulation in *E. huxleyi* have interpreted intracellular CA to be located exclusively in the chloroplast and chloroplast membrane, and absent from the coccolith vesicle and cytoplasm, based on the localization of intracellular CA in diatoms via immunolabeling (Bach et al., 2013). Consequently, the potential role of intracellular CA in the calcification pathway in coccolithophores is unresolved.

Here we propose a new approach to empirically constrain changes in the activity of CA in specific cellular pathways, in particular in carbon pathways to calcification which are particularly relevant for the interpretation of geochemical proxies in coccoliths. We evaluate the potential of a double oxygen and carbon isotope labeling method to estimate CA activity and subsequently constrain DIC fluxes in the cell of the coccolithophore. The double label approach exploits the different behaviors of oxygen and carbon isotopes in the cell: the labeled oxygen isotopes in DIC is progressively lost into the large pool of water by the exchange reaction of oxygen atoms between DIC and water, while the carbon atoms remain trapped in DIC. In a double-label experiment, DIC species are labeled by both heavy carbon and oxygen isotopes, and we measure the amount of label in coccolith calcite over a time course. The amount of carbon label in coccoliths is controlled by the amount of DIC depositing in calcification and the

amount of oxygen label in coccoliths is controlled by both DIC uptake and CA activity. Here we use a multi-component cell model to test the sensitivity of this label technique to different cell configurations. We then apply the model to simulate coccolith carbon and oxygen isotopic compositions from by double-labeling cultures of *E. huxleyi* at two different CO_2 concentrations, to evaluate if different CA concentrations and carbon pumping could be distinguished from the evolution of labeled coccoliths through time.

2. METHODS

2.1. Incubation experiments

2.1.1. Acclimation cultures

Cultures of *E. huxleyi* (strain RCC1258, a pelagic strain isolated off the Portuguese coast in 1998) obtained from Roscoff Culture collection were acclimated to high and low CO_2 concentrations (1437 ± 74 and 191 ± 14 ppm of pCO_2, respectively) by growth in semi-continuous batch cultures for at least 8 generations. Culture media was prepared using 0.2 µm filtered natural seawater (collected in the Gulf Stream off the coast of Florida with salinity of 35), enriched with N, P, vitamins and trace metals according to Price et al. (1988), and sterilized by autoclaving. Then manipulation of the seawater carbon system was achieved by bubbling for at least 12 h with controlled mixtures of air and CO_2 (either 1000 or 150 ppm CO_2) to reach the target pCO_2 conditions, prior to cell inoculation, and maintenance of bubbling during culture. Growth was carried out at 22 °C in culture cabinets (Percival Scientific) equipped with cool white fluorescent tubes (Alto II™ Technology), where photosynthetic active radiation (PAR) was 251 ± 8 µmol photons m^{-2} s^{-1} under a 14:10 h light dark cycle. Three biological replicates (bottle A, B and C) for each CO_2 treatment were grown in 1L polycarbonate bottles, and the cell density was maintained between 2000 and 67,000 cell ml^{-1} during the semi-continuous culture to maintain cells in exponential growth phase.

2.1.2. Incubation of cells with double label

To initiate cells for incubation with isotope label, 1 L polycarbonate bottles were inoculated with three replicate each (A, B, and C) of cells pre-acclimated to each pCO_2 concentration at an initial cell density of ~4000–8000 cell ml^{-1}. Light, growth media, temperature, and CO_2 bubbling were maintained identical to the acclimation cultures. Cell growth during this period was daily monitored using a Beckman Coulter Z2 Coulter Particle Counter and Size Analyzer, and presence of unwanted prokaryotes and eukaryotes were not detected in the cultures during routine examination using a light microscope (OLYMPUS BH 2). This growth rate is not employed in our modeling, because the direct uptake of labeled ^{13}C more precisely constrains calcification rate during the label incubation.

After 4 days, bubbling of cultures was suspended for the label time course. The culture media was enriched with 0.1 mM isotopic labeled DIC. The labelled DIC was previously prepared by dissolving $NaHCO_3$ with 98% ^{13}C

Table 1
Measured results in experiments.

Experiment	Bottle*	Time after labeling (min)	$\delta^{13}C$ (‰, VPDB)		$\delta^{18}O$ (‰, VPDB)		Average growth rate (d^{-1})**	Cell density (num/ml)	POC per cell (pmol)	PIC per cell (pmol)	C/N
			Rep 1	Rep 2	Rep 1	Rep 2					
High CO_2	A	167	244.63	225.19	51.53	46.34		26,610	2.57	0.91	8.7
	B	338	438.48	452.46	53.61	56.54	0.67	33,900	2.21	0.93	10.3
	C	354	425.77	432.60	65.09	67.06		35,375	3.39	1.24	11.18
Low CO_2	A	167	197.09	195.70	185.20	185.87		46,090	2.14	1.1	7.75
	B	214	284.53	279.34	238.11	235.35	0.53	48,900	2.2	1.39	8.24
	B	338	549.32	556.94	330.90	334.19		48,900	2.2	1.39	8.24
	C	181	327.16	286.17	302.49	238.04		65,090	2.06	1.24	8.72
	C	335	551.30	515.25	338.30	316.55		65,090	2.06	1.24	8.72

* The bottle A, B and C are biological replicates during the incubation process to monitor cell growth conditions. During isotope labeling, the cells in bottle A, B and C were harvested at different timings as measured to generate an isotope ratio time series for later parameter fitting in model. Coccolithophores cell density in low CO_2 environment was higher resulting there are enough cells to perform twice analyses in low CO_2 B and C bottles.

** The growth rate is based on cell density measured during the grow-up phase of the labeling experiment.

(Aldrich Chemistry) into H_2O with 97% ^{18}O (Cambridge Isotope Laboratories, Inc.) and overnight equilibration. Incubation with labeled DIC continued for a period between 3 and 5.9 h (details in Table 1). During this time course, aliquots of cell culture (ranging from 160 to 700 ml) were harvested on a 3 μm polycarbonate membrane (Whatman Cyclopore). The estimated number of cells collected on the filter ranged between 7 and 36 million (details in **Table S7**), which corresponds to approximately 106 and 476 μg of inorganic carbon, respectively. The polycarbonate filter was rinsed twice with 5 ml of deionized water under vacuum in order to prevent salt precipitation and then stored at −20 °C until further analysis.

2.2. Laboratory measurements

Culture media DIC was measured at the beginning and the end of the incubation using a membrane inlet mass spectrometer (MIMS; PFEIFFER Vacuum) by acidifying 0.2 μm filtered (Millipore syringe filter) media samples to pH ~4.5 using 2 mM of citric acid buffer and making 4 standard additions of 500 μM DIC. Culture media pH was measured on the total hydrogen ion scale using Thymol Blue with an error of 0.01 (Zhang and Byrne, 1996).

Particulate organic carbon (POC) and particulate organic nitrogen (PON), were determined in samples collected on pre-combusted GF/F filters. After fuming under vacuum for 24 h with HCl to remove carbonate, filters were dried overnight and pressed into tin foil boats. Elemental analysis was performed using a ThermoFisher Flash-EA 1112 coupled with a Conflo IV interface to a ThermoFisher Delta V isotope ratio mass spectrometer (IRMS). Samples were combusted in the presence of O_2 in an oxidation column at 1020 °C. Combustion gases were passed through a reduction column (650 °C), and produced N_2 and CO_2 gases were separated chromatographically and transferred to the IRMS via an open split for on-line isotope measurements. Finally, results were normalized per cell.

For determination of particulate inorganic carbon (PIC, coccolith carbonate), the samples were harvested on polycarbonate membranes. Membranes were inmersed in 2% HNO_3, in order to dissolve calcite. The acid-labile concentration of Ca was measured by Inductively Coupled Plasma Mass Spectrometry (Agilent 8800 ICP-QQQ-MS). The amount of $CaCO_3$ was calculated and normalized per cell, assuming that the contribution of Ca from organic components is negligible.

Carbon and oxygen isotope compositions of the labeled coccolith calcite were measured using a GasBench II coupled to a Delta V mass spectrometer (both ThermoFischer Scientific, Bremen, Germany) as described in Breitenbach and Bernasconi (2011). Culture samples collected on polycarbonate membranes were pre-treated to remove organic components before analysis. For this, samples were soaked for 5 min in methanol and rinsed with deionized water under vaccum. Then a soaking step in oxidizing solution (50% v/v of 3% sodium hypochlorite (NaClO) and 30% hydrogen peroxide (H_2O_2)) for 10 min followed by a rinse with deionized water under vaccum was repeated twice. Finally, the calcite was resuspended in methanol and allowed to evaporate overnight.

About 100 μg of powdered coccolith calcite were placed in vacutainers, previously flushed with helium and were reacted with 5 drops of phosphoric acid at 70 °C. The instrument was calibrated with the international reference materials NBS 19 ($\delta^{13}C = +1.95‰$, $\delta^{18}O = -2.2‰$) and NBS 18 ($\delta^{13}C = -5.01‰$, $\delta^{18}O = -23.00‰$). Reproducibility of the measurements at natural abundance is better than 0.1‰. There are no internationally accepted calcite standards with labeled isotope compositions. However, based on dilution experiments with ^{13}C-enriched glucose measured with an Elemental analyzer coupled to the same instrument type (Glucose Std. 50: calculated $\delta^{13}C = +50‰$, measured $\delta^{13}C = +59.7 \pm 0.3$, $n = 5$; Glucose B476: calculated $\delta^{13}C = +476‰$, measured $\delta^{13}C = 457‰ \pm 0.1$, $n = 2$), we estimate that the accuracy of the ^{13}C-labeled carbon isotope values for values between +100 and +500‰ are within 15‰ of the true values. The isotope ratio units, both for carbon and oxygen, are VPDB in this study.

2.3. Description of the model

In this study we design a 4-box model based on the previously published diatom model by Hopkinson et al. (2011) to simulate the CCMs of *E. huxleyi*. We also perform sensitivity tests to determine which individual processes, such as calcification, bicarbonate pumping and CA activity, can influence the labeling results. A simple summary of all models can be found in **Table S2**. For simulating the experimental data, the model is used to find solutions that simultaneously fit the measured coccolith carbon and oxygen isotope ratios from labeled experiments at different time during the incubation.

Our labeled isotope model includes four compartments, namely the (1) extracellular environment (e), (2) cytoplasm (c), (3) chloroplast (x) and (4) coccolith vescle (v) (Fig. 1**a**). In this model, the input parameters include the seawater DIC (CO_2 and HCO_3^-) concentrations, pH of seawater, cell surface area and cell volume, and the permeability of the cell membrane to CO_2 and HCO_3^-. The initial concentrations of CO_2 and HCO_3^- within the cell were set equal to those of seawater. The variations of DIC in the cell can be caused by three types of processes: (1) the cross membrane transport (diffusion and activity transport), (2) the DIC consumption by photosynthesis and calcification, and (3) reactions between CO_2 and HCO_3^- catalyzed by CA. Details of these processes are given in the following sections and more assumptions in the model can be found in the **supporting information S1** including the initial values of isotope ratios and the effect of cell compartment pH on fitting results. The variation of DIC concentrations with time after label addition was calculated using the ordinary differential equation (ODE) solver, ode15, in Matlab (equations details in **supporting information S2**) within a time range comprised between 0 s and the longest growth time of our labeling experiments (i.e. 2.4×10^4 s). Then the DIC fluxes at each time section were output to calculate the coccolith isotopes after labeling. The unlabeled

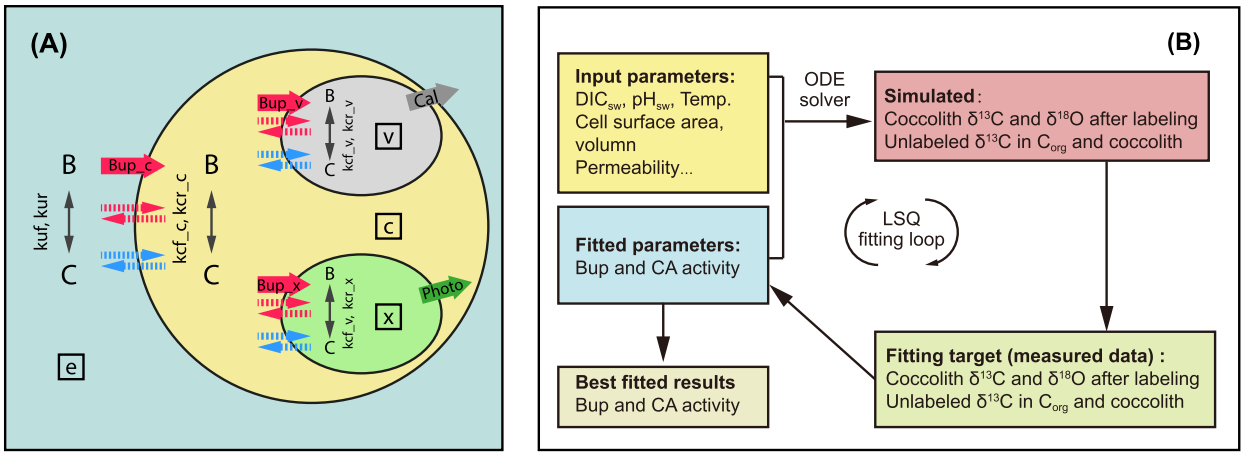

Fig. 1. **A.** Schematics of the 4-box model, showing the pathways, fluxes and interconversion of bicarbonate (B) and CO_2 (C). The four compartments in the model are seawater (e), cytoplasm (c), coccolith vesicle (v) and chloroplast (x). Solid red arrows (B_{up}) represent bicarbonate pumping across membranes, while dashed red and blue arrows are passive diffusion of bicarbonate and CO_2, respectively. Calcification is represented by a solid gray arrow (Cal) and photosynthesis by a solid green arrow (Photo). **B.** Schematics of logic structure of the 4-box model: ODE is ordinary differential equation and LSQ fitting represent least-square fitting. (For interpretation of the references to colour in this figure legend, the reader is referred to the web version of this article.)

coccolithophore carbon isotope fractionations were also calculated providing another constrain on the simulation results (details in **supporting information S3**). To ascertain the optimal model parameters to fit with the measured isotope ratio data over the labeling time course, the system is solved numerically by varying CA activity and bicarbonate pumping rates to minimize the difference between modeled and measured isotope ratio data using the function 'lsqcurvefit' in Matlab (Fig. 1**b**).

2.3.1. Diffusion and active transport rate of DIC species

In our model, we combine the HCO_3^- and CO_3^{2-} together and use the term B; thereby the DIC pool is simplied as C (CO_2) and B (HCO_3^- and CO_3^{2-}, most of B are HCO_3^-). This simplification is valid because acid-base equilibration between HCO_3^- and CO_3^{2-} occurs very rapidly (Zeebe and Wolf-Gladrow 2001). Following Hopkinson et al. (2011), we assume that CO_2 can only diffuse across membranes following the concentration gradient, while HCO_3^- is mainly transported via active pumping, with a small portion being diffused (HCO_3^- permeability is at least 5 order of magnitude lower than that of CO_2, as observed in coccolithophore (Blanco-Ameijeiras et al., 2020).

The diffusion rate of CO_2 and HCO_3^- follows Fick's Law (Eq. (1)). The diffusive in/out flux depends on the permeability (P_{DIC}) and the concentration gradient of both DIC species (CO_2 or bicarbonate) between the two sides of the membrane (G_{DIC}).

$$Flux_{DIC} = P_{DIC} \times G_{DIC} \quad (1)$$

On the other hand, the HCO_3^- pumping rate (Bup) can be described by the Michaelis-Menten equation:

$$Bup = V_{max} \times \frac{[HCO_3^-]}{K_m + [HCO_3^-]} \quad (2)$$

where V_{max} is the maximum pump rate and K_m is the half saturation HCO_3^- concentration. Km is assumed to be 100 μM following Hopkinson et al. (2011), which is much smaller than the HCO_3^- concentration of seawater used in our study. Hence, HCO_3^- uptake rates (Bup) remain always close to the V_{max} value.

2.3.2. Photosynthesis and calcification rate

The gross photosynthesis rate is a Michaelis-Menten process, which depends on the number of functional Ribulose-1,5-bisphosphate Carboxylase/Oxygenase (RubisCO) per cell ($N_{RubisCO}$), the turnover rate of one RubisCO protein ($k_{cat\_RubisCO}$) and the CO_2 concentration in the chloroplast:

$$Photo = N_{RubisCO} \times k_{cat\_RubisCO} \times \frac{[CO_2]}{K_{m\_ph} + [CO_2]} \quad (3)$$

where K_{m_ph} is the half saturation concentration of CO_2 in photosynthesis. Using a RubisCO mass of 560 kDa (Ma et al., 2009) and a bulk RubisCO turnover rate of 0.66 μmol min^{-1} mg^{-1} (Boller et al., 2011), we calculate that one RubisCO protein can fix 6.16 CO_2 molecules in one second ($k_{cat\_RubisCO} = 6.16$ CO_2 s^{-1}). For *E. huxleyi*, Boller et al. (2011) estimated that the RubisCO half saturation concentration, K_{m_ph}, was 72 μM, and therefore we use this value in our model construction.

There are no available published data on the RubisCO numbers per cell ($N_{Rubisco}$). Therefore, here we calculate this parameter by assuming that RubisCO accounts for about 4% of total cellular protein (Losh et al., 2013), and that the protein density ($\rho_{protein}$ with a unit of protein copies per um^3) in algae is $\sim 3 \times 10^6$ μm^{-3} (Milo, 2013). The CO_2 concentration in low CO_2 condition is close to the present ocean environment and the settings in Losh et al. (2013). Thereby, we employed these number directly to estimate RubisCO per cell in low CO_2 experiment. Given an *E. huxleyi* cell radius (r) of 2.5 μm as we measured in the low CO_2 environment, the number of RubisCO per cell growing at low CO_2 concentrations can be estimated by:

$$N_{\mathrm{Rubisco}}(LC) = \frac{4}{3} \times r^3 \times \rho_{protein} \times 4\% \times \frac{1}{N_A} \approx 1.3 \times 10^{-17}\ mol \quad (4)$$

where N_A is the Avogadro's constant. The C:N ratio and organic carbon per cell (POC) at high CO_2 concentrations are higher than those at low CO_2 (Table 1) and a higher C:N ratio represents less protein per cell. If we assume that the mole fraction of RubisCO percentage is constant (4%) in high and low CO_2 conditions, the number of RubisCO per cell (N_{Rubisco}) under high CO_2 calculated by Eq.5 is ~25% lower (1.0×10^{-17} mol per cell) than that calculated by Eq. (4) for lower CO_2 conditions:

$$N_{\mathrm{Rubisco}}(HC) = N_{\mathrm{Rubisco}}(LC) \times \frac{C{:}N_{LC}}{C{:}N_{HC}} \times \frac{POC_{HC}}{POC_{LC}} \approx 1.0 \times 10^{-17}\ mol \quad (5)$$

The calcification rate (Cal) was set as a function of gross photosynthesis rate (Photo), net photosynthesis ratio (R_{net}) and PIC:POC ratio, rather than as a dynamic function of carbonate saturation. R_{net} is defined as the ratio between net photosynthesis rate and Photo (Eq. (7)).

$$Cal = Photo \times R_{net} \times PIC : POC \quad (6)$$

$$R_{net} = \frac{Net\ \ photosynthesis\ \ rate}{Photo} \quad (7)$$

2.3.3. CA activity

The CA enzyme catalyzes the hydration and dehydration reactions between CO_2 and HCO_3^-. The CO_2 and HCO_3^- exchanging rate including catalyzed hydration reaction rate and uncatalyzed hydration/hydroxylation rate can be described by the following equations:

$$exchaing\ \ rate = k_{uf} \times [CO_2] + k_{cat\_CA} \times [CA] \times \frac{[CO_2]}{K_{m\_hy} + [CO_2]} \quad (8)$$

$$k_{uf} = k_{+1} + k_{+4} \times [OH^-] \quad (9)$$

$$ln^{(k_{+1})} = 1246.98 - \frac{6.19 \times 10^4}{T} - 183.0 \times ln^{(T)} \quad (10)$$

$$k_{+4} = 4.70 \times 10^7 \times e^{(-\frac{2.32 \times 10^4}{RT})} \# \quad (11)$$

where k_{uf} is the uncatalyzed exchanging rate constant (here we combine the uncatalyzed hydration and hydroxylation rate constant into one parameter), k_{cat_CA} is the turnover rate of carbonic anhydrase and K_{m_hy} is the half saturation concentration of CO_2 and the [CA] is CA concentration. R is the gas constant with a value of 8.314 J mol^{-1} K^{-1}. The definition of reaction rate constants, k_{+1} and k_{+4}, are following Zeebe and Wolf-Gladrow (2001). The Eq. (10) and (11) are from Johnson (1982).

Since K_{m_hy} is much larger than the CO_2 concentration in the cell, we can simplify the hydration rate in Eq.8 as:

$$exchanging\ \ rate \approx \left(k_{uf} + \frac{k_{cat\_CA}}{K_{m\_hy}} \times [CA]\right) \times [CO_2] = k_{cf} \times [CO_2] \quad (12)$$

where the k_{cf} is the catalyzed CO_2 hydration rate constants, respectively. Following Uchikawa and Zeebe (2012), we assume that the $\frac{k_{cat\_CA}}{K_{m\_hy}}$ ratio takes the value of 2.7×10^7 M^{-1} s^{-1}.

The dehydration rate constant (k_{cr}) can be calculated using the catalyzed CO_2 hydration rate constant (k_{cf}) using the following equation:

$$k_{cr} = k_{cf} \times F_B \times \frac{[H^+]}{K_1} \quad (13)$$

where the F_B is the ratio of $HCO_3^-/(HCO_3^- + CO_3^{2-})$, $[H^+]$ is the concentration of hydrogen, and K_1 is the first carbonic acid dissociation constant. Since we assumed that there are only two species of DIC (CO_2 and HCO_3^-), here the effect of CO_3^{2-} should be calibrated.

$$F_B = \frac{1}{1 + \frac{K_2}{[H^+]}} \quad (14)$$

where K_2 is the second carbonic acid dissociation constant. K_1 and K_2 can be calculated by temperature, pressure and salinity (Lueker et al., 2000). The uncatalyzed dehydration rate constant (k_{ur}) can be calculated by k_{uf} and pH in culture medium in the similar method as Eq. (13).

2.4. Sensitivity analysis on labeled experiments

Before running full simulations on the 4-box model, it is useful to isolate the influence of individual processes on the carbon and oxygen isotope ratios of the labeled experiments. These processes include 1) calcification and photosynthesis rate, 2) CA activity, 3) bicarbonate pumping, 4) uncatalyzed DIC reaction rate which depends on seawater pH, and uncatalyzed DIC reaction rate constants. To isolate these processes, we simplify the original '4-box' model to three simpler box-models, namely, '2-box', '3-box-cx' and '3-box-cv', and carry out sensitivity tests of each process separately. The detailed parameter configurations can be found in **supporting information S4**.

3. RESULTS OF MEASUREMENT AND SENSITIVITY TESTS

3.1. Growth, calcification, and incorporation of double label at high and low CO_2

During the 4-day grow up of cells before labeling, the growth rate under the two experimental conditions were similar, 0.53 d^{-1} and 0.62 d^{-1} for the low CO_2 and high CO_2 treatments, respectively. The particulate inorganic carbon and particulate organic carbon ratio (PIC:POC in mol/mol) was higher (0.59) in the low CO_2 experiment than in the high CO_2 experiment (0.33). The POC per cell in the high CO_2 experiment is 2.72 pmol/cell (1 pmol = 10^{-12} mol), about 20% higher than that in the low CO_2 experiment (2.13 pmol/cell).

Following addition of the isotope label, the time course evolution of coccolith carbon isotope ratios though time was similar in both low CO_2 and high CO_2 experiments. The labeled coccolith carbon isotope ratios increase with sampling time ranging from 193‰ at 2.78 h to 515‰ at 5.9 h. reflecting the progressive uptake of labeled DIC by the cell and a progressively higher fraction of cellular calcite produced post-addition of the label. However, the coccolith labeled oxygen isotope ratios in these two experiments were quite different. The heavy oxygen isotope was lost faster from DIC into water in the high CO_2 experiment than in the low CO_2 experiment, resulting in much lower $\delta^{18}O$ in the high CO_2 experiment (Fig. 3). The results of model

sensitivity tests are presented to provide context for interpretation of the labeled data in these experiments.

3.2. Basic sensitivity of labels to different parameters in models

A cascade of the simplified 2-box and 3-box models is used to diagnose the influence of the calcification rate, DIC uptake, CO_2 leakage from chloroplast, and the location of CA, on the coccolith oxygen and carbon isotope ratios after labeling. Because both labels employ the heavy isotope, an increased abundance of the isotope label is manifest as an increase in coccolith $\delta^{13}C$ and $\delta^{18}O$. Because isotope ratios of labeled DIC are 3–4 orders of magnitude larger than the cellular fractionation (e.g. the 1‰ fractionation of carbon in calcification and the −25 to −11‰

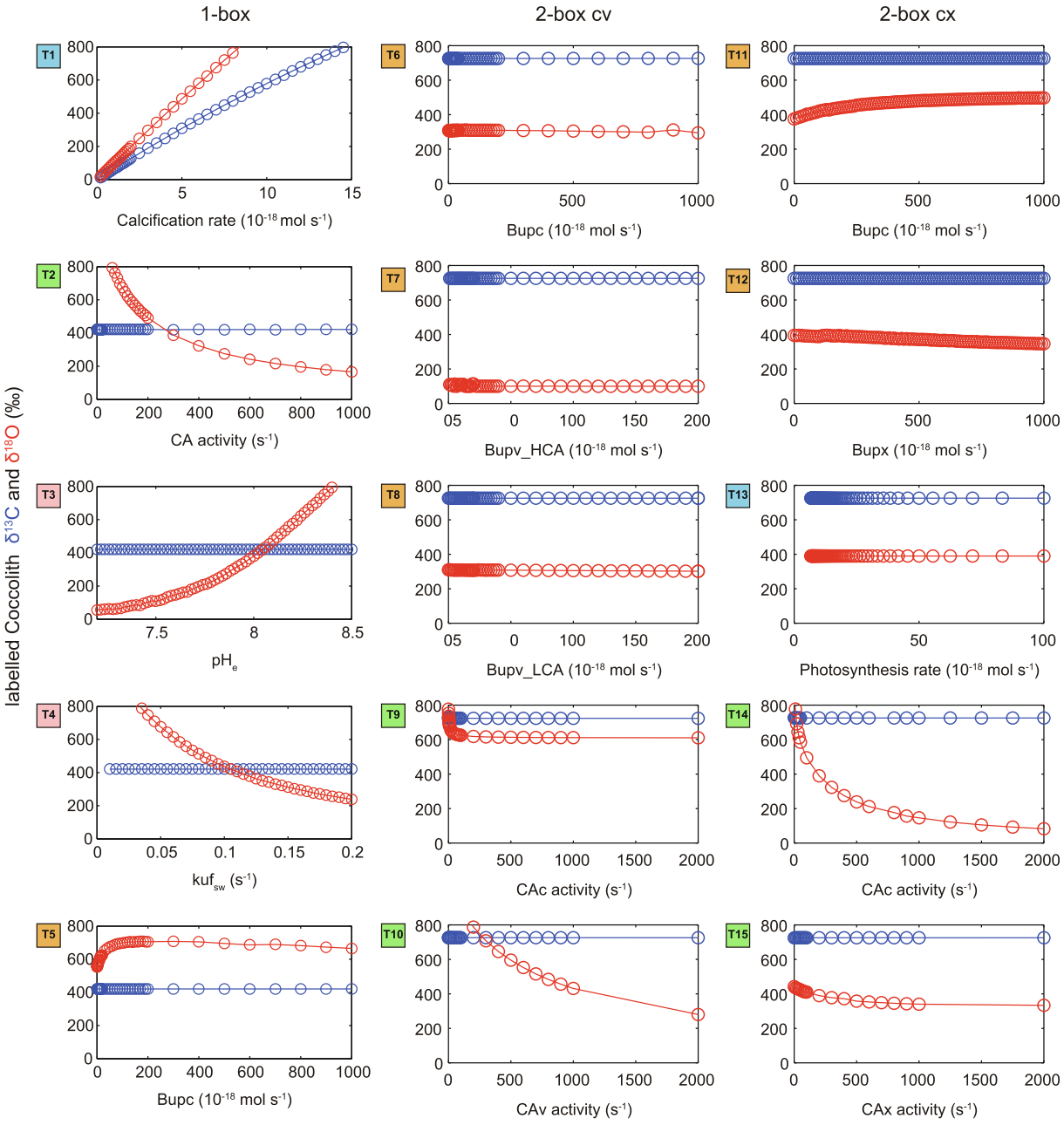

Fig. 2. The results of 15 sensitivity tests: coccolith carbon (blue) and oxygen (red) isotope ratio 6 hours after adding labeled DIC are plotted against the varied parameters (the whole time series can be found in Supporting information). The results in first column are from the '2-box model', those in the second column are from the '3-box cv model' and those in the third column are from the '3-box cx model'. The test numbers with blue background represent sensitivity tests on carbon sinks in the cell. Those with green background are tests on CA activities in different compartments. Those with pink background are tests on the DIC reactions process. Those with yellow background are tests on bicarbonate pumping. (For interpretation of the references to colour in this figure legend, the reader is referred to the web version of this article.)

Table 2
Labeled carbon and oxygen isotope response to different processes: '↑' represents the isotope increases with the increase of different processes rate, '↓' represents the isotope decreases with the increase of different processes rate '↑↓' represents the response of isotope is not monotonous with the variation of process and '—' represent the labeled isotope in coccolith is not sensitive to the process.

Increased processes	Labeled C isotope	Labeled O isotope	Parameter name in model
Calcification rate	↑	↑	Cal
CA activity	—	↓	k_{cf}
Uncatalyzed DIC reaction rate	—	↓	k_{uf}, pH_e
HCO_3^- uptake	—	↑↓	V_{max}
Photosynthesis rate	—	—	Photo

fractionation of carbon in photosynthesis), the isotopic signals discussed in this paper refer exclusively to those created by the addition of isotopically heavy ^{18}O and ^{13}C label. The trends in $\delta^{13}C$ and $\delta^{18}O$ described here are unique to the labeled experiment, and do not describe the natural response of coccolith $\delta^{13}C$ and $\delta^{18}O$ as a result to physiological fractionation processes. The results of sensitivity tests can be found in Fig. 2 and **Fig. S2** in supplementary and the influences of different processes on labeled isotope of coccolith are summarized in Table 2. Overall, the coccolith carbon isotope ratio after labeling is a function of calcification rate, while the oxygen isotope evolution is controlled by calcification rate, CA activity in the DIC pathway to the calcification site, and uncatalyzed DIC reaction rate in the culture medium.

3.2.1. Calcification and photosynthesis rate

Based on the result of sensitivity test **T1**, which was performed by the '2-box' model as the description in the **supporting information S2**, we found that both carbon and oxygen isotope ratios in labeling are sensitive to the calcification rate. The increase of calcification rate can always lead to increases in $\delta^{13}C$ and $\delta^{18}O$ (Fig. 2-T1). This model simulates the experimental approach of introducing a label into an actively growing, but not decalcified, culture of coccolithophores, a technique used to avoid altering cell physiology due to decalcifying treatments. With this approach, the coccoliths harvested though time after labeling are a mixture of both labeled and unlabeled coccoliths. With a fixed amount of unlabeled coccoliths, if the calcification rate during the labeling experiment is higher, there will be more coccoliths with extreme heavy isotope enrichment causing an increase in $\delta^{13}C$ and $\delta^{18}O$. Moreover, the following sensitivity tests show other process play minor role in coccolith carbon isotope ratios (see the following sections), so that the carbon isotope ratio can provide an accurate estimation of calcification/growth rate during the short duration (hours) of the labeling experiment. The results of **T13** show photosynthesis rate has no impact on coccolith $\delta^{18}O$ or $\delta^{13}C$ under the conditions of proposed label experiment (Fig. 2-T13).

3.2.2. CA activity and localization

The effects of CA in different compartments were tested in **T2** (cytoplasm CA by model '2-box'), **T9** (cytoplasm CA by model '3-box-cv'), **T10** (coccolith vesicle CA by model '3-box-cv'), **T14** (cytoplasm CA by model '3-box-cx') and **T15** (chloroplast CA by model '3-box-cx'). The results suggest that when the CA activity increases, no matter where it was located, the coccolith $\delta^{18}O$ will always decrease due to loss of the label from the DIC to water, but the $\delta^{13}C$ is unaffected by CA. However, location of the CA does affect the magnitude of the $\delta^{18}O$ response to CA. Only when the CA is located in the model site of calcification, which is the cytoplasm in **T2** and **T14**, and the coccolith vesicle in **T10**, does the coccolith $\delta^{18}O$ can keep decrease to the minimum value of ~40‰ (Fig. 2-T2**, T10, T14**). Otherwise, when the enhanced CA appears in the non-calcification compartment, such as in the test **T9**, even when the CA activity of cytoplasm increases to as high as $1 \times 10^6\ s^{-1}$ (about three order of magnitude higher than the fitted value), the oxygen isotope ratio of coccolith still remains about 600‰ and does not decrease further (Fig. 2-T9).

3.2.3. Uncatalyzed DIC exchange rate

In the sensitivity tests **T3** and **T4**, we used uncatalyzed hydration rate constant (k_{uf}) from $0.01\ s^{-1}$ to $0.20\ s^{-1}$ and an extracellular pH (pH_e) ranging from 7.2 to 8.5. The results show that if the pH_e decreases or the k_{uf} increase, the $\delta^{18}O$ will decrease (Fig. 2**-T3, T4**). Both of these factors cause a higher uncatalyzed hydration rate, resulting in a faster loss of the labeled oxygen from DIC to water prior to uptake into the cell. We also note that only the seawater uncatalyzed hydration rate plays an important role in oxygen isotope ratios. The dynamics of cellular pH won't change the oxygen isotope significantly because of the small cell volume compared with the culture medium (**supporting information S7**).

3.2.4. Bicarbonate pumping rate's effect

The roles of bicarbonate pumping were tested in **T5**, **T6**, **T7**, **T8**, **T11** and **T12**. Bicarbonate pumping does not affect the coccolith $\delta^{13}C$ and affects coccolith $\delta^{18}O$ in a complex manner. (1) When the bicarbonate uptake rate on the cell membrane is close to zero, the coccolith $\delta^{18}O$ increases with increasing pumping rate. That is because an enhanced bicarbonate uptake rate across the cytoplasmic membrane (Bup_c) can pump more labeled HCO_3^- into the cell. (2) At the other extreme situation, when the Bup_c rate is very high, the extreme high Bup_c will cause a huge increase of DIC concentration in the cell. The hydration or dehydration rate depends not only on the CA activity, but also the concentration of DIC. So, an extreme high Bup_c rate will cause a faster loss of label into water, resulting a comparatively lower $\delta^{18}O$ in coccoliths. (3) Contrasting effects of bicarbonate pumping into the chloroplast and coccolith

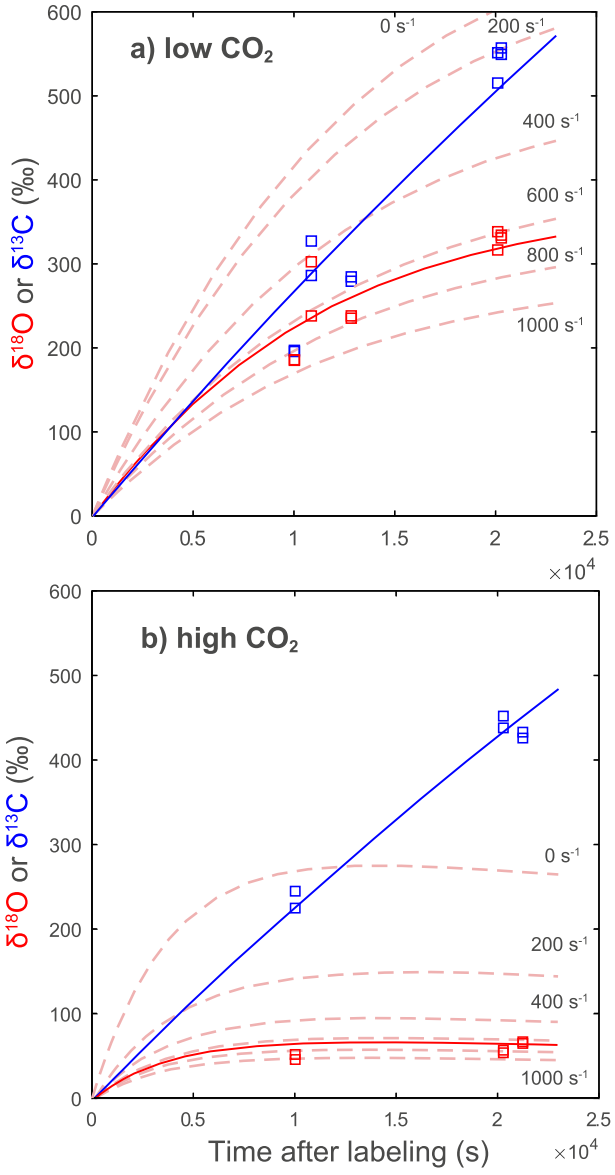

Fig. 3. The carbon and oxygen isotopic ratios of coccoliths over the time course following addition of isotope label, as measured (squares) and in simulations (lines, by 4-box model). The red lines and squares are oxygen isotope and the blues ones are carbon isotope ratio. The pink dashed lines represent modeled oxygen isotope ratio when CA activity in cytoplasm increases from 0 s^{-1} to 1000 s^{-1} with an increment of 200 s^{-1}. (For interpretation of the references to colour in this figure legend, the reader is referred to the web version of this article.)

vesicle are simulated. In the results of **T7**, **T8** and **T12**, we find the $\delta^{18}O$ decreases slightly with the increase of the bicarbonate uptake rate into the chloroplast (Bup_x) or with the decrease of the bicarbonate uptake rate into the coccolith vesicle (Bup_v). When the Bup_x increases or the Bup_v decreases, more labeled DIC is pumped into chloroplast compared with the amount of labeled DIC pumped into coccolith vesicle. To summarize, the bicarbonate pump rate can change the $\delta^{18}O$ of labeled coccoliths, but this effect is not constant nor significant compared with the effects of calcification rate, CA activity and the uncatalyzed DIC reaction rate.

4. CONSTRAINTS OF CA AND CARBON FLUXES FROM A SAMPLE LABEL EXPERIMENT

4.1. Simulation of the observed isotopic data in labeled calcite experiments

For this experimental dataset, we use the measured DIC concentration of seawater, pH of seawater, temperature, cell surface area, organic carbon per cell and PIC:POC ratio as input parameters. Some parameters can be found directly or estimated indirectly from previous studies, such as the photosynthesis and respiration ratio, and RubisCO turnover rate. Other parameters, such as the intercellular pH, the RubisCO number per cell are estimated as described in the **Methods**. In this fitting, we also put the carbon isotope fractionation in coccolith and C_{org} ($\varepsilon_{coccolith\text{-}HCO3}$ and $\varepsilon_{HCO3\text{-}corg}$) into consideration. For carbon isotope ratios in the organic carbon, we analyzed the sample from the same growth conditions in unlabeled condition. For the coccolith isotope vital effect, we assume unlabeled composition similar to literature values of 0.5 and −0.5‰ for low CO_2 condition and high CO_2 condition, respectively (McClelland et al., 2017; Stoll et al., 2019), showing values of $\varepsilon_{coccolith\text{-}HCO3}$ as 1.5 and 0.5. All input parameters and fitted results can be found in Table 3. The results of DIC concentration and carbon flux in the coccolithophore cells are shown in Fig. 4. It should be noted that the chloroplast CO_2 concentrations in our simulation did not approach the saturated concentration for RubisCO, although previous observation of RubisCO amounts in *E. huxleyi* suggested that near-saturating CO_2 at RubisCO was required to attain measured photosynthesis rates (Losh et al., 2013). One reason may be that there is no pyrenoid in our model, in which the protein shell and small volumn can decrease the CO_2 efflux and maintain a much higher CO_2 concentration around RubisCO (Hopkinson et al., 2011).

4.1.1. CA activity in cytoplasm and coccolith vesicle

The increasingly depletion of coccolith $\delta^{18}O$ though time following addition of the label, cannot be achieved by our model only using the rate of uncatalyzed exchange of isotopes between DIC and water (Fig. 3). The low $\delta^{18}O$ values in the coccoliths, compared to the initial DIC, requires CA to be present in the direct pathway to calcification, e.g. in the cytoplasm and/or coccolith vesicle. This contrasts with the model of Bach et al. (2013) who proposed intracellular CA location only in the chloroplast, and not in the cytoplasm, because in diatoms the βCA in diatoms is located to the chloroplast and the δCA on the plasma membrane. Our results require either that the recognized CA transcripts in *E. huxleyi* may correspond to CA located instead or additionally in the cytoplasm and coccolith vesicle, or that additional CA forms, not recognized in previous transcriptomics of *E. huxleyi*, are located in the cytoplasm and coccolith vesicle. The growing diversity of proteins with

Table 3
Input parameters and output results in the 4-box model simulations.

Input parameters	Definitions	Low CO_2	High CO_2	Comments
$\delta^{13}C_{DIC(t=0)}$	Initial DIC carbon isotope ratio	−2.81	−2.81	Measured*
$\delta^{18}O_{DIC(t=0)}$	Initial DIC oxygen isotope ratio	−0.57	−0.57	Measured
DIC_{sw} (μM) **	seawater DIC concentration	1803 ± 11	2395 ± 51	Measured
pHe	seawater pH	8.29 ± 0.0	7.58 ± 0.1	Measured
pHc	cytoplasm pH	8.09	7.38	Calculated by pHe − 0.2 following Suffrian et al. (2011)
pHv	coccolith vesicle pH	8.23	8.23	Holtz et al. (2017)
pHx	chloroplast pH	7.90	7.90	Anning et al. (1996)
T (℃)	culture temperature	22	22	Measured
k_{uf} (s^{-1})	uncatlyzed DIC reaction rate	0.0616	0.0340	Zeebe and Wolf-Gladrow (2001)
k_{cfv} (s^{-1})	catalyzed DIC reaction rate constant in coccolith vesicle	100–500	100–500	Given
k_{cfx} (s^{-1})	catalyzed DIC reaction rate constant in chloroplast	100–500	100–500	Given
P_C (cm s^{-1})	CO_2 permeability	6.13E-03	6.13E-03	Blanco-Ameijeiras et al. (2020)
P_B (cm s^{-1})	HCO_3^- permeability	2.70E-07	2.70E-07	Blanco-Ameijeiras et al. (2020)
Cell_SA (cm^2)	Cell surface area	1.37E-06	1.37E-06	Measured
PIC:POC	cell PIC:POC ratio	0.59	0.33	Measured
Corg per cell (pmol)		2.133	2.723	Measured
C:N	Organic carbon and nitrogen ratio	8.23	10.06	Measured
R_{net}	Net photosynthesis rate: Gross photosynthesis	0.75	0.75	Kottmeier et al. (2016)
RubisCO per cell (mol)		1.3E-17	1.1E-17	Estimated from Milo (2013)
Fitted results***		Low CO_2	High CO_2	
V_{max_c} (10^{-17} mol s^{-1})	Maximum HCO_3^- pumping rate into cytoplasm	1.72 ± 0.60	0.69 ± 0.16	The value after '±' is one standard deviation of fitting results
V_{max_x} (10^{-17} mol s^{-1})	Maximum HCO_3^- pumping rate into chloroplast	10.2 ± 0.66	1.3 ± 0.92	
V_{max_v} (10^{-17} mol s^{-1})	Maximum HCO_3^- pumping rate into coccolith vesicle	0.63 ± 0.04	0.57 ± 0.03	
CA_c (kcf_c, s^{-1})	catalyzed DIC reaction rate constant in cytoplasm	647 ± 132	952 ± 186	
kap (s^{-1})	Apparent CA activity	947 ± 124	1275 ± 96	
$\varepsilon_{coccolith\text{-}HCO3}$ ****	coccolith carbon isotope fractionation from DIC	1.41 (1.50)	0.51 (0.50)	Values in brackets are fitting targets (from literature)
$\varepsilon_{HCO3\text{-}Corg}$	C_{org} carbon isotope fractionation from DIC	20.22 (17.9)	30.52 (35.8)	Values in brackets are fitting targets (from measurement); equal with $\varepsilon_p = 10.1$ and 23 in this case;
CO_2/HCO_3^- net influx		0.39 (27.9% CO_2)	3.10 (75.6% CO_2)	
Ce/Cc		1.24	1.06	
Cx/Ce		3.65	0.88	

* The carbon and oxygen isotope of unlabeled DIC in the seawater could be altered slightly after CO_2 bubbling. But these initial values do not have significant impact on the fitting results.
** This DIC measured concentrations are the averaged values of three bottles at the beginning and at the end of labeling experiment. About 50 μmol DIC was consumed by calcification and photosynthesis during the labeling experiment. That's the reason why the [DIC] in this table are ~50 μmol lower than those in Fig. 4.
*** This fitting is based on the assumption that CA activities in the coccolith vesicle and chloroplast equal to 100 s^{-1}.
**** Notice $\varepsilon_{coccolith\text{-}HCO3}$ is different with coccolith vital effect ($VE_{coccolith}$), which is always defined as the carbon isotope difference between coccolith and non-biogenic carbonate, $VE_{coccolith} \approx \varepsilon_{coccolith\text{-}HCO3} - 1$.

recognized CA functionality (e.g. Jensen et al., 2019) attests to the potential for operation of forms in coccolithophores which have not yet been recognized by transcriptomics.

In our simulations, no significant difference in the CA activities in cytoplasm low CO_2 experiment (647 ± 132 s^{-1}) and high CO_2 experiment (952 ± 186 s^{-1}) is

required to match the data in our label experiment. Our estimated CA activities are in the upper range of the hydration rate constant catalyzed by CA in diatoms, 50–500 s^{-1}) depending on the seawater DIC concentration (Fig. 5, Hopkinson et al., 2011). Previous cellular models of coccolithophores have made varying assumptions about intracellular CA activity. One model assumed a CA concentration in each compartment ranging from 0.1 to 1 mol m^{-3}, equivalent to k_{cf} ranging from 270 to 2700 s^{-1} (McClelland et al., 2017). Another model assumed that the reaction rate of DIC exchanging in the cell is 1000 times larger than that in natural seawater (when pH = 8.3), equivalent to a CA activity of about 142 s^{-1} in (Holtz et al., 2015). The absolute CA activity inferred by the 4-box model here is somewhat dependent on the assumptions of other model parameters, but for no alternate parameter choices did we find a significant difference in CA activities between the low CO_2 and high CO_2 treatments. The model-inferred cytoplasm CA activity decreases with any increase of modeled CA activity in other compartments (**supporting information S6**). For the standard four-compartment model, the CA activity in coccolith vesicle and chloroplast were fixed as 100 s^{-1} in these fittings because at this activity the CA in chloroplast and coccolith vesicle is saturated for CCM. If we used the 2-box model to estimate the apparent CA activity (k_{ap}) which represents the total intracellular CA activity (**supporting information S5**), then the fitting results show that in the low CO_2 condition, the coccolithophore k_{ap} is 947 ± 124 s^{-1}, while the k_{ap} in high CO_2 condition is about 1275 ± 96 s^{-1}; i.e. also no significant difference in total CA activity among the different treatments. The fitting results of bicarbonate pumping rates on different membrane do not show a significant trend with the increase of CA activity (**Fig. S6** a, c).

If the main function of CA was enhancing the CCM, then we would expect a decrease in CA activity in high CO_2 treatment. If this is true, it could be possible that small changes in CA activities is not detected by the precision of the double label technique. However, transcriptomics run in *E. huxleyi* grown under treatments most similar to ours (DIC 2000–2200 μM; CO_2aq treatments of 38 and 10 μM), transcriptomics also revealed no significant (e.g. distinct at 2 standard error) differences in the expression of αCA1, αCA2, γCA or δCA. Differences in βCA could not be assessed due to lack of replicates to estimate standard errors (Bach et al., 2013). Although transcript abundance is not a direct quantification of CA, it is generally assumed to reflect the cellular demand for specific proteins (Bach et al., 2013), so the transcriptomics results are consistent with our findings of no differences of CA activities between low and high CO_2 treatments. Furthermore, Rost

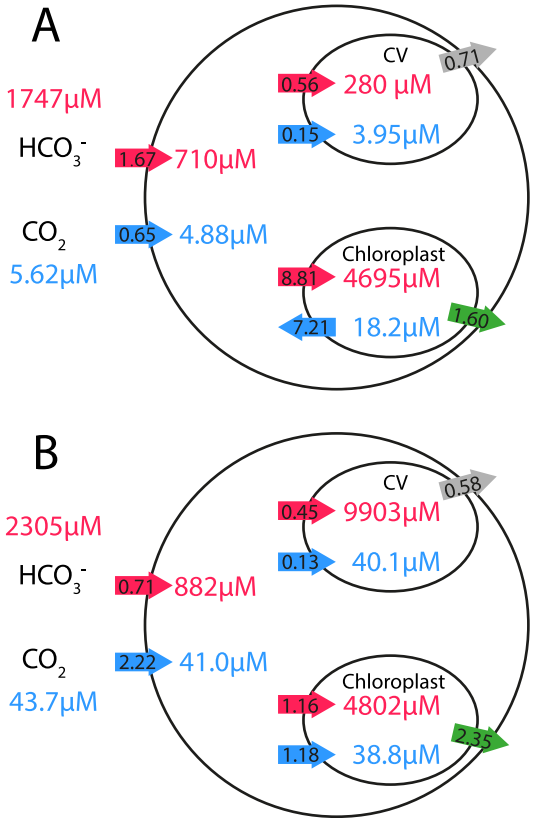

Fig. 4. The cell DICs concentrations and fluxes in two CO_2 environments. The blue arrows are CO_2 flux, the red arrows are HCO_3^- flux, the gray arrows are calcification rate and the green arrows are photosynthesis rate. The direction of arrows represents the DIC net flux goes from one box into the other box. The numbers in arrow are with unit of flux is 10^{-17} mol s^{-1} $cell^{-1}$. Note that the DIC concentrations in this figure are slightly higher than those listed in Table 3, which is caused by calcification and photosynthesis usage of carbon. (For interpretation of the references to colour in this figure legend, the reader is referred to the web version of this article.)

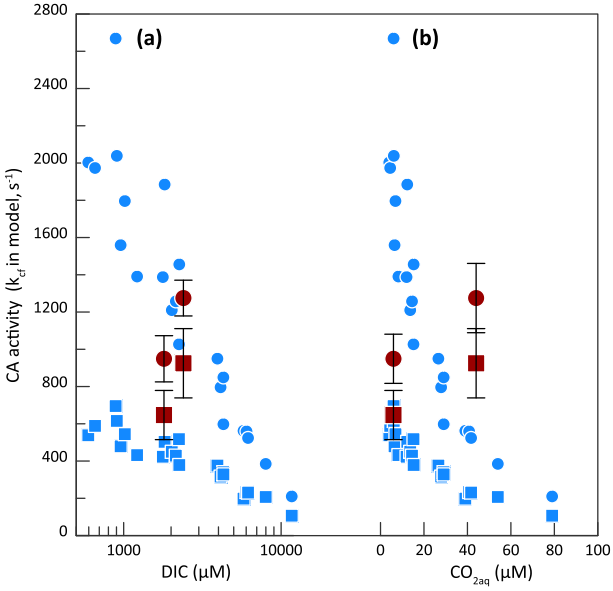

Fig. 5. The variations of CA activities with DIC concentration. The error bars represent one standard division in fitting. The red dots are apparent CA activity and red squares are simulated CA activity by the 4-box model. The blue dots and squares are diatom apparent CA activity and cytoplasm CA activity (Hopkinson et al., 2011). (For interpretation of the references to colour in this figure legend, the reader is referred to the web version of this article.)

et al. 2003 found that internal CA concentration of *E. huxleyi* did not change when cultured under a wide range of CO2 concentrations (36–1800 ppm). Increasing the CCM efficiency may not be the only role of the CA inside cell, and other cellular processes may require similar CA activity in both high and low CO_2 conditions. The CA plays important roles in adjusting the pH in both plants (e.g. Furla et al., 2000) and animals (Stewart et al., 1999). The cell may need to increase the CA activity for the cellular pH or calcification. Moreover, as mentioned above, the estimation of CA activity in our model gives the information about the total CA activity. The enhanced CA activity (compared with the saturated CA activity) in high CO_2 environment may be not only in the cytoplasm but also can be in the coccolith vesicle. Previous studies emphasized the influence of carbon system on coccolithophore's calcification (e.g. Beaufort et al., 2011). The first explanation could be that, in high CO_2 environment, the coccolithophore may produce more CA to maintain the calcification site pH and, thereby keep the carbonate saturation.

The second explanation may concern the energy budget between CCM and nutrient uptake. In a two years culture of another key species of coccolithophore, *Gephyrocapsa oceanica*, Jin et al. (2013) found that the C:N ratio decreased and organic nitrogen per cell increased in long term high CO_2 environment and they suggested that, in high CO_2 environment, the energy spent in CCM could be used in the nutrient uptake resulting in a low C:N ratio. In our culture, there should be no limitation for coccolithophores in neither energy (enough light) nor nutrient (enough nitrogen and phosphate for low cell density batch cultures). Therebefore, perhaps a pressure to downregulate the CA at high CO_2, to conserve energy for nutrient acquisition, is alleviated in our nutrient replete cultures.

The third explanation is that these CA activities in our treatments are normal values for coccolithophores or the decrease of CO_2 is not enough for coccolithophores to increase the CA activity. Strong upregulation of many CA transcripts was observed in treatments in which DIC was 1200 μM or lower, conditions in which there were also upregulation of RubisCO and bicarbonate exchangers (Bach et al., 2013). In our culture setting, the low CO_2 conditions featured a DIC concentration of about 1800–1900 μM, similar to ocean conditions from the late Pleistocene to the pre-industrial period (Zeebe, 2012). Therefore, while the CO_2 setting in our experiment is low, the DIC concentration may not be low enough for coccolithophore to enhance the CA activity significantly, especially in the light and nutrient replete conditions of our cultures. Further information might be gained from experimental conditions in which nutrients are limited.

4.1.2. Bicarbonate pumping rate

Inverse modeling of oxygen isotopic composition evolution time course, in combination with the ^{13}C label time course constraint on carbon uptake rate during the incubation, suggest a significant difference in the bicarbonate pumping rate into the cell and chloroplast between high and low CO_2 treatments. The bicarbonate net flux into the chloroplast (Bup_x) increases from 1.3×10^{-17} mol s^{-1} $cell^{-1}$ in high CO_2 condition to about 10.2×10^{-17} mol $s^{-1}cell^{-1}$ in low CO_2 condition. This result is constrained primarily by the dependence of photosynthetic rate on the CO_2 in the chloroplast and the observed ^{13}C incorporation rates. Under low CO_2, the bicarbonate pumping rate into the cell (Bup_c) also increases by more than 2-fold, from 0.69×10^{-17} mol s^{-1} $cell^{-1}$ in high CO_2 condition to about 1.72×10^{-17} mol s^{-1} $cell^{-1}$ in low CO_2 conditions, respectively. In the low CO_2 experiment, the net CO_2/HCO_3^- influx into cell is about 0.39, equivalent to 27.9% CO_2, while this ratio is about 3.10, equivalent to 75.6% CO_2 uptake, in the high CO_2 experiment. This variation of influx ratio is consistent with the calculation in Kottmeier et al. (2016) based on MIMS analysis, in which the HCO_3^- influx to the cell increases in a low CO_2 environment.

In contrast to the case for the chloroplast and cell, the bicarbonate pumping rate into coccolith vesicle does not require significant change between the two CO_2 conditions to match the available constraints here. As bicarbonate has very low passive membrane permeability, and our model specifies no active efflux of bicarbonate from the coccolith vesicle except via precipitation into calcite, the net DIC influx is modeled to match calcification rate less the CO_2 influx. There is a negligible change in the CO_2:HCO_3^- transport ratio into the coccolith vesicle between the high and low CO_2 treatments, with 80% C import as HCO_3^-. Somewhat surprisingly, the inverse model solution also implies a significantly lower DIC concentration in the coccolith vesicle in the low CO_2 treatment. Indeed, if in the coccolith vesicle, the Ca^{2+} concentration was comparable to that of seawater and pH were maintained 8.23, the inferred DIC for our low CO_2 experiment would lead to undersaturation of a bulk calcification fluid with respect to calcite. A similar undersaturation was simulated by the model assumptions of (McClelland et al., 2017). However, a further sensitivity test (supporting information, Fig. S7) shows that the DIC concentration in coccolith vesicle increases with the increase of coccolith vesicle pH. In the low CO_2 experiment, if coccolith vesicle pH is 8.4, instead of our default value of 8.23, the DIC concentration of the coccolith vesicle increases from 200 μM to 1100 μM, further increase of pH to 8.8 leads to DIC in excess of 2000 μM. This underscores the sensitivity of DIC concentration, and potentially the calcite saturation state, on the pH in coccolith vesicle and may suggest that the coccolithophore adjust the coccolith vesicle pH for calcification.

In this model, the calcification rate is set externally and is independent of the availability of substrates in the coccolith vesicle. It would be ideal to constrain the DIC concentration and pH in the coccolith vesicle via a dynamic calcification rate, analogous to the dynamic photosynthesis rate which depends on the CO_2 concentration in the chloroplast attained through both CO_2 diffusion and bicarbonate pumping. The calcification rate could be expected to depend on the supply of Ca and DIC, or potentially on the oversaturation state of $CaCO_3$ in the coccolith vesicle, determined by the Ca concentration, DIC concentration, and vesicle pH (e.g. as simulated in Holtz et al. (2015); (2017;))). While modeling such a dynamic calcification

routine would be desirable, a realistic representation of the calcification process in coccolithophores is currently limited by both major gaps in understanding of calcification pathway as well as by lack of observations. A classic representation of calcification rate in aqueous media would define a rate dependence on the free $[Ca^{+2}]$ $[CO_3^{-2}]$ ion activity product (IAP). However, the fraction of DIC as CO_3^{-2} depends very strongly on pH (when pH = 8, about 18% DIC are in the form of CO_3^{2-}, while this number increases to 85% when the pH = 9). Moreover, there are no robust observational constraints on the regulation of the pH in the coccolith vesicle. More recent ion by ion growth models suggest that both HCO_3^- and CO_3^{-2} participate in calcite growth and the growth rate depends additionally on the ratio of Ca^{+2}: CO_3^{-2} (e.g. Wolthers et al., 2012; Watkins et al., 2014). A further complication is the unknown delivery mechanisms of Ca to the calcification site. It may be possible that Ca is accumulated in the endoplasmic reticulum or Golgi body, complexed to P (Gal et al., 2016) before delivery to the calcification vesicle. Therefore, the free Ca concentration may be a small part of total Ca supply for calcification. Subsequently, in the coccolith vesicle, during the initial phases of biomineralization, Ca is accreted on organic macromolecular sites which are part of the template for coccolith biomineralization, before any mineral is precipitated and any CO_3^{-2} ion is aggregated (Gal et al., 2016). Given these complexities, it is not clear during what, if any, phase of coccolith assembly a conventional "bulk fluid" aqueous composition might be confidently applied to predict calcification rate.

4.2. Implications for geochemical proxies

This label experiment provides empirical evidence for the presence of CA in the calcification pathway of coccolithophores, in contrast to some earlier models of cellular carbon pathways (Bach et al., 2013). The presence of CA has important implications for the equilibration of natural abundance isotopes of oxygen between DIC and water, which in turn affects the interpretation of oxygen isotope ratios in coccolith carbonate. Abiogenic calcite growth experiments show that the presence of CA maintains $\delta^{18}O$ equilibrium between water and DIC species, and this equilibrium is reflected in the calcite (Thaler et al., 2017; Watkins et al., 2013; 2014). Notably, in experiments in which isotopically light CO_2 was supplied to the reaction, the presence of CA precluded the inheritance of this light CO_2 oxygen in the precipitated calcite, which instead maintained a composition at equilibrium with the water (Watkins et al., 2014).

Several models have been proposed to explain variations in $\Delta^{18}O_{coccolith\text{-}water}$ at a given temperature. One model suggested that coccoliths inherit the oxygen isotopic composition of all dissolved carbon species according to their relative abundance at calcification pH (Ziveri et al., 2012), similar to a model suggested for planktic foraminifera (Zeebe, 1999). Another model suggests that variation in $\Delta^{18}O_{coccolith\text{-}water}$ results from isotopic disequilibrium between H_2O and DIC prior to calcification, due to calcification rates from an internal carbon pool which exceeded the rate of isotopic re-equilibration of the internal DIC pool with H_2O (Hermoso et al., 2014; Hermoso et al., 2016a, 2016b; Hermoso, 2015).

The results presented here indicate that a significant CA activity exists in the cellular DIC pathway to calcification. The exchange or cycling times before calcification or photosynthesis from the inferred CA activity can be calculated as:

$$Cycling\ \ times \approx \frac{Cal+Photo}{CO_2 \times k_{ap}} \quad (15)$$

From uptake into the cell, the DIC will undergo about 7.7 and 12.4 hydration/dehydration cycles in low and high CO_2, respectively, before it is deposited as calcite or transformed into organic carbon. In principle, CA activities in different coccolithophores may contribute to the range of $\Delta^{18}O_{coccolith\text{-}water}$ among different species, and in a given species under varying experimental conditions. The enhancement of DIC-H_2O equilibration by CA in coccolithophores in the calcification pathway must therefore be accounted for in future conceptual and quantitative models of $\Delta^{18}O$coccolith-water. Likewise, the presence of dissolved CA should accelerate clumped isotope equilibrium in the bulk solution, and be accounted for in future models of clumped isotope behavior in coccoliths. Moreover, the role of CA activity in algal CCMs has a potential to explain the coupling of carbon and oxygen isotope vital effect observed in coccoliths since the Miocene by Bolton and Stoll (2013) and Bolton et al. (2016). Here we propose that further refinement of cellular models could target well-constrained culture data to make a next step in improving our understanding of coccolith oxygen isotope vital effect.

5. CONCLUSIONS AND FUTURE WORK

The novel double isotope label (oxygen and carbon) method described here, detecting the time evolution of label incorporation in coccolith calcite, is shown to be a sensitive approach to evaluate the significance of CA in the calcification pathway, complementing transcriptomics techniques which identify upregulation of CA but not its location or function/pathway. A 4-box model is developed to infer the sensitivity of the isotope labels to CA abundance in different cellular pathways and to different bicarbonate pumping rates. Using the 4-box model, we calculate the CA activity in cytoplasm which is sufficient to saturate the CCM, a threshold which depends on the relationship of bicarbonate pumping rate into chloroplast and cytoplasm.

The application of the double label method to derive a time evolution of the label abundance in coccolith calcite allowed us to evaluate the significance of CA in the calcification pathway of *E. huxleyi* under high and low CO_2 conditions. The result shows that CA is present in the calcification pathway in both treatments. In our experiments, there is no evidence that coccolithophores increase the CA activity in low CO_2. Since CA can alter the DIC oxygen isotope ratio by accelerating the oxygen atom exchanging rate between DIC and water, we suggest that the activity of CA may be crucial for correct modeling and interpretation of coccolith oxygen isotope fractionation and clumped isotopes in coccoliths.

The isotope label technique and 4-box model provide new insights into DIC fluxes within the cell, and emphasize the importance of CA activity in coccolithophore's CCM, and can therefore clarify the "black box" of coccolithophores' intracellular carbon transport. The method would be applicable to other species of coccolithophores. In future experiments, the precision of estimated CA activity could be improved by more frequent sampling in the first 150 minutes following labeling, by precise pre-label determination of the natural abundance isotopic fractionation of calcite and organic carbon under experimental conditions, and development to detect label abundance in photosynthetically rapidly synthesized products. Further information about the intracellular pH, to date not well constrained (Anning et al., 1996; Suffrian et al., 2011; Holtz et al., 2017), will also improve model precision because intracellular pH affects the rate of uncatalyzed exchange reactions and therefore the fraction of reaction rate attributed to CA.

Declaration of Competing Interest

The authors declare that they have no known competing financial interests or personal relationships that could have appeared to influence the work reported in this paper.

ACKNOWLEDGEMENTS

This study was supported by the Swiss National Science Foundation (Award 200021_182070 to HMS), ETH core funding, the US National Science Foundation (OPP 1744760 to BMH), the National Natural Science Foundation of China (41930536 to CL) and Chinese Scholarship Council (CSC) scholarship to HZ. We sincerely thank two reviewers and editors' suggestions to improve the manuscript.

AUTHOR CONTRIBUTIONS

BH conceived of the double label approach, SBA carried out labeling experiments, SB oversaw measurement of isotope labeled samples; HZ developed the numerical model with guidance from BH and HMS; HZ and HMS wrote the paper with input from other authors.

DATA SECTION

All data are listed in Table 2 and Table 3. The codes of model are available by email request to HZ (103443_rui@tongji.edu.cn).

APPENDIX A. SUPPLEMENTARY MATERIAL

Supplementary data to this article can be found online at https://doi.org/10.1016/j.gca.2020.09.008.

REFERENCES

Anning T., Nimer N., Merrett M. J. and Brownlee C. (1996) Costs and benefits of calcification in coccolithophorids. *J. Mar. Syst.* **9**, 45–56.

Bach L. T., Mackinder L. C., Schulz K. G., Wheeler G., Schroeder D. C., Brownlee C. and Riebesell U. (2013) Dissecting the impact of CO2 and pH on the mechanisms of photosynthesis and calcification in the coccolithophore *Emiliania huxleyi*. *New Phytol.* **199**, 121–134.

Beaufort L., Probert I., de Garidel-Thoron T., Bendif E., Ruiz-Pino D., Metzl N., Goyet C., Buchet N., Coupel P. and Grelaud M. (2011) Sensitivity of coccolithophores to carbonate chemistry and ocean acidification. *Nature* **476**, 80–83.

Blanco-Ameijeiras S., Stoll H. M., Zhang H. and Hopkinson B. M. (2020) Influence of temperature and CO2 on plasma-membrane permeability to CO2 and HCO3- in the marine haptophytes *Emiliania huxleyi* and *Calcidiscus leptoporus* (Prymnesiophyceae). *J. Phycol.*. https://doi.org/10.1111/jpy.13017. Accepted Author Manuscript.

Boller A. J., Thomas P. J., Cavanaugh C. M. and Scott K. M. (2011) Low stable carbon isotope fractionation by coccolithophore RubisCO. *Geochim. Cosmochim. Acta* **75**, 7200–7207.

Bolton C. T., Hernandez-Sanchez M. T., Fuertes M. A., Gonzalez-Lemos S., Abrevaya L., Mendez-Vicente A., Flores J. A., Probert I., Giosan L., Johnson J. and Stoll H. M. (2016) Decrease in coccolithophore calcification and CO2 since the middle Miocene. *Nat. Commun.* **7**, 10284.

Bolton C. T. and Stoll H. M. (2013) Late Miocene threshold response of marine algae to carbon dioxide limitation. *Nature* **500**, 558–562.

Bown P. (1998) *Calcareous nannofossil biostratigraphy*. Kluwer Academic, Chapman and Hall.

Breitenbach S. F. and Bernasconi S. M. (2011) Carbon and oxygen isotope analysis of small carbonate samples (20 to 100 µg) with a GasBench II preparation device. *Rapid Commun. Mass Spectrom.* **25**, 1910–1914.

Diez Fernández S., Ruiz Encinar J., Sanz-Medel A., Isensee K. and Stoll H. M. (2015) Determination of low B/Ca ratios in carbonates using ICP-QQQ. *Geochem. Geophys. Geosyst.* **16**, 2005–2014.

Furla P., Allemand D. and Orsenigo M.-N. (2000) Involvement of H+-ATPase and carbonic anhydrase in inorganic carbon uptake for endosymbiont photosynthesis. *Am. J. Physiol.-Regulatory, Integrative Comparative Physiol.* **278**, R870–R881.

Gal A., Wirth R., Kopka J., Fratzl P., Faivre D. and Scheffel A. (2016) Macromolecular recognition directs calcium ions to coccolith mineralization sites. *Science* **353**, 590–593.

Herfort L., Thake B. and Roberts J. (2002) Acquisition and use of bicarbonate by *Emiliania huxleyi*. *New Phytol.* **156**, 427–436.

Hermoso M. (2015) Control of ambient pH on growth and stable isotopes in phytoplanktonic calcifying algae. *Paleoceanography* **30**, 1100–1112.

Hermoso M., Chan I. Z. X., McClelland H. L. O., Heureux A. M. C. and Rickaby R. E. M. (2016a) Vanishing coccolith vital effects with alleviated carbon limitation. *Biogeosciences* **13**, 301–312.

Hermoso M., Horner T. J., Minoletti F. and Rickaby R. E. M. (2014) Constraints on the vital effect in coccolithophore and dinoflagellate calcite by oxygen isotopic modification of seawater. *Geochim. Cosmochim. Acta* **141**, 612–627.

Hermoso M., Minoletti F., Aloisi G., Bonifacie M., McClelland H. L. O., Labourdette N., Renforth P., Chaduteau C. and Rickaby R. E. M. (2016b) An explanation for the 18O excess in Noelaerhabdaceae coccolith calcite. *Geochim. Cosmochim. Acta* **189**, 132–142.

Holtz L.-M., Wolf-Gladrow D. and Thoms S. (2017) Stable carbon isotope signals in particulate organic and inorganic carbon of coccolithophores–A numerical model study for *Emiliania huxleyi*. *J. Theor. Biol.* **420**, 117–127.

Holtz L. M., Wolf-Gladrow D. and Thoms S. (2015) Numerical cell model investigating cellular carbon fluxes in *Emiliania huxleyi*. *J. Theor. Biol.* **364**, 305–315.

Hopkinson B. M. (2014) A chloroplast pump model for the CO 2 concentrating mechanism in the diatom Phaeodactylum tricornutum. *Photosynth. Res.* **121**, 223–233.

Hopkinson B. M., Dupont C. L., Allen A. E. and Morel F. M. M. (2011) Efficiency of the CO2-concentrating mechanism of diatoms. *Proc. Natl. Acad. Sci.* **108**, 3830–3837.

Hopkinson B. M., Dupont C. L. and Matsuda Y. (2016) The physiology and genetics of CO2 concentrating mechanisms in model diatoms. *Current Opinion in Plant Biology* **31**, 51–57.

Jensen E. L., Clement R., Kosta A., Maberly S. C. and Gontero B. (2019) A new widespread subclass of carbonic anhydrase in marine phytoplankton. *ISME J.* **13**(8), 2094–2106. https://doi.org/10.1038/s41396-019-0426-8.

Jin P., Gao K. and Beardall J. (2013) Evolutionary responses of a coccolithophorid Gephyrocapsa oceanica to ocean acidification. *Evolution* **67**, 1869–1878.

Johnson K. S. (1982) Carbon dioxide hydration and dehydration kinetics in seawater 1. *Limnol. Oceanogr.* **27**, 849–855.

Kottmeier D. M., Rokitta S. D., Tortell P. D. and Rost B. (2014) Strong shift from HCO3 − to CO2 uptake in *Emiliania huxleyi* with acidification: new approach unravels acclimation versus short-term pH effects. *Photosynth. Res.* **121**, 265–275.

Kottmeier D. M., Rokitta S. D. and Rost B. (2016a) Acidification, not carbonation, is the major regulator of carbon fluxes in the coccolithophore *Emiliania huxleyi*. *New Phytol.* **211**, 126–137.

Kottmeier D. M., Rokitta S. D. and Rost B. (2016b) H^+-driven increase in CO2uptake and decrease in HCO3− uptake explain coccolithophores' acclimation responses to ocean acidification. *Limnol. Oceanogr*.

Liu Y. W., Eagle R. A., Aciego S. M., Gilmore R. E. and Ries J. B. (2018) A coastal coccolithophore maintains pH homeostasis and switches carbon sources in response to ocean acidification. *Nat. Commun.* **9**, 2857.

Losh J. L., Young J. N. and Morel F. M. (2013) Rubisco is a small fraction of total protein in marine phytoplankton. *New Phytol.* **198**, 52–58.

Lueker T. J., Dickson A. G. and Keeling C. D. (2000) Ocean pCO2 calculated from dissolved inorganic carbon, alkalinity, and equations for K1 and K2: validation based on laboratory measurements of CO2 in gas and seawater at equilibrium. *Mar. Chem.* **70**, 105–119.

Ma Z., Cooper C., Kim H.-J. and Janick-Buckner D. (2009) A study of rubisco through western blotting and tissue printing techniques. *CBE—Life Sci. Ed.* **8**, 140–146.

Mangan N. M., Flamholz A., Hood R. D., Milo R. and Savage D. F. (2016) pH determines the energetic efficiency of the cyanobacterial CO2 concentrating mechanism. *Proc. Natl. Acad. Sci.* **113**, E5354–E5362.

McClelland H. L., Bruggeman J., Hermoso M. and Rickaby R. E. (2017) The origin of carbon isotope vital effects in coccolith calcite. *Nat Commun* **8**, 14511.

Medlin L., Sáez A. G. and Young J. R. (2008) A molecular clock for coccolithophores and implications for selectivity of phytoplankton extinctions across the K/T boundary. *Mar. Micropaleontol.* **67**, 69–86.

Mercado J. M., Ramírez T., Cortés D. and Liger E. (2009) Effect of carbonic anhydrase inhibitors on the inorganic carbon uptake by phytoplankton natural assemblages. *J. Phycol.* **45**(1), 8–15. https://doi.org/10.1111/j.1529-8817.2008.00617.x.

Milo R. (2013) What is the total number of protein molecules per cell volume? A call to rethink some published values. *BioEssays* **35**, 1050–1055.

Müller M. N., Lebrato M., Riebesell U., Barcelos e Ramos J., Schulz K. G., Blanco-Ameijeiras S., Sett S., Eisenhauer A. and Stoll H. M. (2014) Influence of temperature and CO2 on the strontium and magnesium composition of coccolithophore calcite. *Biogeosciences* **11**, 1065–1075.

Nimer N. A., Guan Q. and Merrett M. J., et al. (1994) Extra- and intra-cellular carbonic anhydrase in relation to culture age in a high-calcifying strain of *Emiliania huxleyi* Lohmann. *New Phytologist.* **126**(4), 601–607.

Nimer N. A., Ling M. X. and Brownlee C., et al. (1999) Inorganic carbon limitation, exofacial carbonic anhydrase activity and plasma membrane redox activity in marine phytoplankton species. *J. Phycol.* **35**(6), 1200–1205.

Price N. M., Harrison G. I., Hering J. G., Hudson R. J., Nirel P. M. V., Palenik B. and Morel F. M. M. (1988) Preparation and chemistry of the artificial algal culture medium Aquil. *Biol. Oceanogr.* **6**, 443–462.

Quinn P., Bowers R. M., Zhang X., Wahlund T. M., Fanelli M. A., Olszova D. and Read B. A. (2006) cDNA microarrays as a tool for identification of biomineralization proteins in the coccolithophorid *Emiliania huxleyi* (Haptophyta). *Appl. Environ. Microbiol.* **72**, 5512–5526.

Rost B., Riebesell U., Burkhardt S. and Sültemeyer D. (2003) Carbon acquisition of bloom-forming marine phytoplankton. *Limnol. Oceanogr.* **48**, 55–67.

Soto A. R., Zheng H., Shoemaker D., Rodriguez J., Read B. A. and Wahlund T. M. (2006) Identification and preliminary characterization of two cDNAs encoding unique carbonic anhydrases from the marine alga *Emiliania huxleyi*. *Appl. Environ. Microbiol.* **72**, 5500–5511.

Stewart A., Boyd C. and Vaughan-Jones R. (1999) A novel role for carbonic anhydrase: cytoplasmic pH gradient dissipation in mouse small intestinal enterocytes. *J. Physiol.* **516**, 209–217.

Stojkovic S., Beardall J. and Matear R. (2013) CO2-concentrating mechanisms in three southern hemisphere strains of E miliania huxleyi. *J. Phycol.* **49**, 670–679.

Stoll H., Langer G., Shimizu N. and Kanamaru K. (2012) B/Ca in coccoliths and relationship to calcification vesicle pH and dissolved inorganic carbon concentrations. *Geochim. Cosmochim. Acta* **80**, 143–157.

Stoll H. M., Guitian J., Hernandez-Almeida I., Mejia L. M., Phelps S., Polissar P., Rosenthal Y., Zhang H. and Ziveri P. (2019) Upregulation of phytoplankton carbon concentrating mechanisms during low CO2 glacial periods and implications for the phytoplankton pCO2 proxy. *Quat. Sci. Rev.* **208**, 1–20.

Stoll H. M. (2005) Limited range of interspecific vital effects in coccolith stable isotopic records during the Paleocene-Eocene thermal maximum. *Paleoceanography* **20**, PA1007.

Stoll H. M. and Schrag D. P. (2001) Sr/Ca variations in Cretaceous carbonates: relation to productivity and sea level changes. *Palaeogeogr. Palaeoclimatol. Palaeoecol.* **168**, 311–336.

Suffrian K., Schulz K. G., Gutowska M. A., Riebesell U. and Bleich M. (2011) Cellular pH measurements in *Emiliania huxleyi* reveal pronounced membrane proton permeability. *New Phytol.* **190**, 595–608.

Thaler C., Millo C., Ader M., Chaduteau C., Guyot F. and Ménez B. (2017) Disequilibrium δ18O values in microbial carbonates as a tracer of metabolic production of dissolved inorganic carbon. *Geochim. Cosmochim. Acta* **199**, 112–129.

Uchikawa J. and Zeebe R. E. (2012) The effect of carbonic anhydrase on the kinetics and equilibrium of the oxygen isotope exchange in the CO2–H2O system: Implications for δ18O vital

effects in biogenic carbonates. *Geochim. Cosmochim. Acta* **95**, 15–34.

von Dassow P., Ogata H., Probert I., Wincker P., Da Silva C., Audic S., Claverie J.-M. and de Vargas C. (2009) Transcriptome analysis of functional differentiation between haploid and diploid cells of *Emiliania huxleyi*, a globally significant photosynthetic calcifying cell. *Genome Biol.* **10**, R114.

Watkins J. M., Hunt J. D., Ryerson F. J. and DePaolo D. J. (2014) The influence of temperature, pH, and growth rate on the δ18O composition of inorganically precipitated calcite. *Earth Planet. Sci. Lett.* **404**, 332–343.

Watkins J. M., Nielsen L. C., Ryerson F. J. and DePaolo D. J. (2013) The influence of kinetics on the oxygen isotope composition of calcium carbonate. *Earth Planet. Sci. Lett.* **375**, 349–360.

Wolthers M., Nehrke G., Gustafsson J. P. and Van Cappellen P. (2012) Calcite growth kinetics: Modeling the effect of solution stoichiometry. *Geochim. Cosmochim. Acta* **77**, 121–134.

Zeebe R. E. (1999) An explanation of the effect of seawater carbonate concentration on foraminiferal oxygen isotopes. *Geochim. Cosmochim. Acta* **63**, 2001–2007.

Zeebe R. E. and Wolf-Gladrow D. (2001) *CO2 in seawater: equilibrium, kinetics, isotopes*. Gulf Professional Publishing.

Zeebe R. E. (2012) History of Seawater Carbonate Chemistry, Atmospheric CO2, and Ocean Acidification. *Annu. Rev. Earth Planet. Sci.* **40**, 141–165.

Zhang H. and Byrne R. H. (1996) Spectrophotometric pH measurements of surface seawater at in-situ conditions: absorbance and protonation behavior of thymol blue. *Mar. Chem.* **52**, 17–25.

Ziveri P., Stoll H., Probert I., Klaas C., Geisen M., Ganssen G. and Young J. (2003) Stable isotope 'vital effects' in coccolith calcite. *Earth Planet. Sci. Lett.* **210**, 137–149.

Ziveri P., Thoms S., Probert I., Geisen M. and Langer G. (2012) A universal carbonate ion effect on stable oxygen isotope ratios in unicellular planktonic calcifying organisms. *Biogeosciences* **9**, 1025–1032.

Associate editor: Claire Rollion-Bard